WO_3/TiO_2 composite multi-layer photoanode based dye sensitized solar cells: promoting electron injection process

LI WENQIN*, LIU HUI, FAN WENPU, YUAN FENG, WU ZIHUA
School of Environmental and Materials Engineering, Shanghai Engineering Research Center of Advanced Thermal Functional Materials, College of Engineering, Shanghai Polytechnic University, Shanghai 201209, China

Dye-sensitized solar cells are promising alternative photovoltaics because of environmentally friendly features. Nanocrystalline TiO_2, used as electron-transporting layer in DSSCs, plays an important role in exciton separation and charge injection process. However, its relatively low electron diffusion coefficient hampered further optimization using pure TiO_2 film as photoanode electrode. Accordingly, a narrow bandgap WO_3 electron transport layer along with a negative conduction band edge was introduced on the bottom of the traditional TiO_2 film to promote electron injection process. DSSCs with 540 nm WO_3 and TiO_2 multi-layer exhibits the best short-circuit current density of 13.04 mA/cm^2 and photoelectric conversion efficiency of 5.39%, 40% higher compared to the traditional configured devices.

(Received December 3, 2020; accepted June 11, 2021)

Keywords: Amorphous tungsten oxide, Electron transporting layer, Photoanode, DSSCs

1. Introduction

Since the first report of dye-sensitized solar cell (DSSCs) by Brian O'Regan and Michael Grätzel in 1991, [1] dye-sensitized solar cells have attracted worldwide attention because of their relatively low cost, good stability, simple process, and abundant material sources [2-6]. Typical dye-sensitized solar cells are sandwich structures composed of photoanode, photocathode and electrolyte, in which semiconductor oxides in photoanode play an important role in dye adsorption process and photo-generated carrier separation and injection process [3]. An efficient photoanode electron transport layer can deliver the photo-generated electrons into conduction band efficiently, which can effectively slow down the recombination of injected electrons with the oxidized dye or with I_3^- in electrolyte, thus improving the photovoltaic conversion efficiency [6]. Up to now, many semiconductor oxides with excellent electron transport properties, such as TiO_2, ZnO, SnO_2, etc., have been developed as photoanode materials for solar cells [7, 8]. Amongst, the anatase TiO_2 is a semiconductor compound with large band gap (Eg=3.2 eV) and shows good electron transport performance in DSSCs [9, 10]. However, the relatively low electron diffusion coefficient makes it difficult to optimize the photovoltaic conversion performance using pure TiO_2 film as photoanode electrode both in DSSCs and pervoskite solar cells [11, 12]. Many physical and chemical strategies were used to reduce the interface charge accumulation. For instance, doping of TiO_2 anodes with metallic elements (such as Cu, Sn, Ni, Ag and Zn, etc.) may create an additional energy barrier on the TiO_2 surface, which is beneficial to suppression of electron recombination and depression of the dark current [13-17]. Besides, photon upconversion through rare earth ions (such as Er^{3+}, Sm^{3+}, Nd^{3+}, etc.) [18-22] provides an alternative approach to improve the performance of the DSSCs by converting unutilized sub-bandgap NIR photons into visible photons. Compared with the aforementioned modification strategies, tuning the free energy (ΔG) between the functional interfaces by simply inserting an inorganic modification layer is a more facile method to boost interfacial charge transfer process. Tungsten oxide is a typical n type semiconductor oxide with quantum size effect and excellent electron transport ability. More importantly, the bandgap of tungsten oxide is a bit narrower with respect to TiO_2 with a value around 2.7eV [23, 24]. And the conduction band edge for tungsten oxide is -5.24eV, slightly negative with respctive to that of TiO_2 -4.21eV [25]. The unique bandgap and conduction band edge alignment between tungsten oxide and TiO_2 may create an additional ΔG to drive the charge injection into the FTO substrate, which is favorable to inhibition of charge recombination. Accordingly, a series of WO_3/TiO_2 composite multilayer photoanode were prepared and applied in DSSCs to boost the electron injection process. The morphology and optical properties of the film were analyzed by scanning electron microscopy (SEM) and UV-Vis absorption spectroscopy. The results indicated that the introduction of WO_3 film is beneficial to dye adsorption process. The electron lifetime was significantly improved which is beneficial to charge injection process.

Consequently, the DSSCs based on 540 nm WO_3/TiO_2 hybrid electron transport layer achieved a power conversion efficiency of 5.39%, an increment of 36% was realized with respect to pure TiO_2 electron transport layer.

2. Experimental

2.1. Materials and characterization

Sensitizer TG6 (Fig. 1) was purchased from Shanghai Institute of Ceramics, Chinese Academy of Sciences. Other starting materials were commercially purchased and without any further purification. The absorption spectra were measured by Shimadzu UV2550 spectrophotometer, with scanning range of 350 nm ~ 800 nm. Scanning electron microscope (SEM) was characterized by FEI Magellan 400. The structure of WO_3 was characterized by X-ray diffraction (XRD) using a Bruker D8 Discover diffractometer. The photovoltaic performance was measured with Keithley 2400 digital source meter under illumination of the Solar IV 150A solar simulator. Cell active area was controlled to be 0.16 cm^2 with a metal mask. The electrochemical impedance spectra (EIS) were completed by CHI660E electrochemical workstation under dark using two-electrode system. The EIS spectra were scanned in a frequency range of 0.1 Hz~100 kHz with applied bias potential set at the open circuit voltage of the solar cells. The alternate current (AC) amplitude was set at 10 mV.

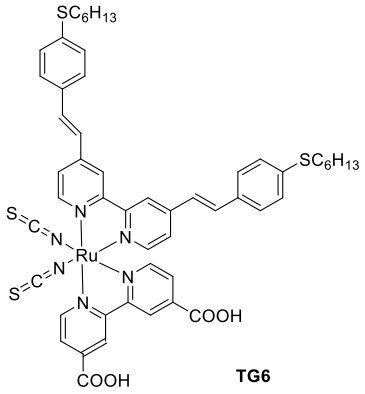

Fig. 1. Molecular structure of TG6

2.2. Preparation of precursor sol for tungsten oxide

Tungstic acid (5g) was dissolved in 35 mL 30% hydrogen peroxide and stirred for 1h at 95 °C to obtain a transparent solution. A mixture contained 50 mL ethanol and 40 mL distilled water were added dropwise and further stirred for another 20 min to obtain a colorless precursor sol.

2.3. Fabrication of dye-sensitized solar cells

The FTO conductive glass was washed thoroughly and exposed under ultraviolet radiation for 15 min. The FTO glass was preheated to 450 °C and different amount of peroxytungstic acid sol was uniformly sprayed onto the top of glass conductive surface to obtain a series of precursor film. The films were annealed at 450°C for 30 min. A TiO_2 film composed of 3μm nanocrystalline TiO_2 layer and 4 μm scattering layer was prepared ontop of WO_3 film and treated following the literature [26]. A pure TiO_2 photoanode were prepared separately as blank reference. The resulting films were placed into a dimethyl sulfoxide (DMSO) and ethanol mixture contained 0.3 mmol/L of TG6 dye and 10 mmol/L of CDCA overnight to obtain dye sensitized photoanodes. The counter electrodes were platinum plated glass electrodes. In this work, 0.1 mol/L LiI, 0.05 mol/L I_2, 0.60 mol/L BMII (1-butyl-3-methylimidiazolium iodide) and 0.60 mol/L tert-TBP in acetonitrile was used as the redox electrolyte.

3. Results and discussion

3.1. SEM images and XRD pattern

WO_3 film was prepared on the surface of FTO glass by facile spray pyrolysis with oxotungstic acid precursor sol. The XRD spectra of the sample after annealing was presented in Fig. 2. The diffraction analysis indicated the sample obtained was mainly crystalline WO_3, corresponding to monoclinic phases according to JCPDS 42-1260. Whereas diffraction peaks located at 24.40°, 34.17°, and 54.93° can be assigned to the (200), (220), and (420) lattice planes. To study surface morphology of WO_3 film, SEM analysis was carried out from the top-view. As shown in SEM images of Fig. 3a and 3b, the WO_3 film was uniformly coated onto the FTO substrate without obvious agglomeration. The uniform coverage is favorable to well interaction between WO_3 film and the upper TiO_2 electron transport layer. The cross-sectional SEM images of Fig. 3c-3f revealed that the tungsten oxide was well-aligned against the FTO glass substrate with a thickness of 180 nm, 360 nm, 540 nm and 720 nm, which can be fine controlled through different amount of spray source solutions.

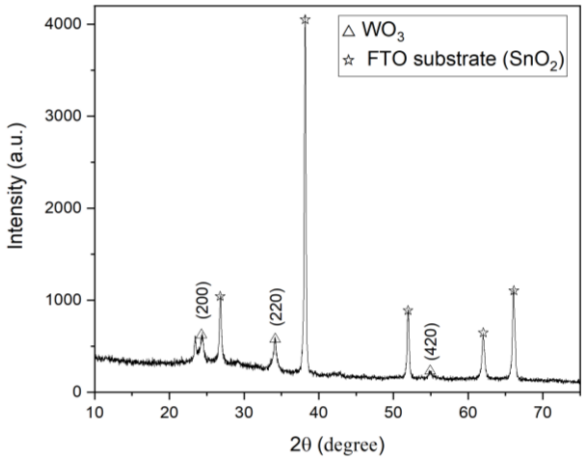

Fig. 2. XRD spectra of tungsten oxide films on top of FTO substrate

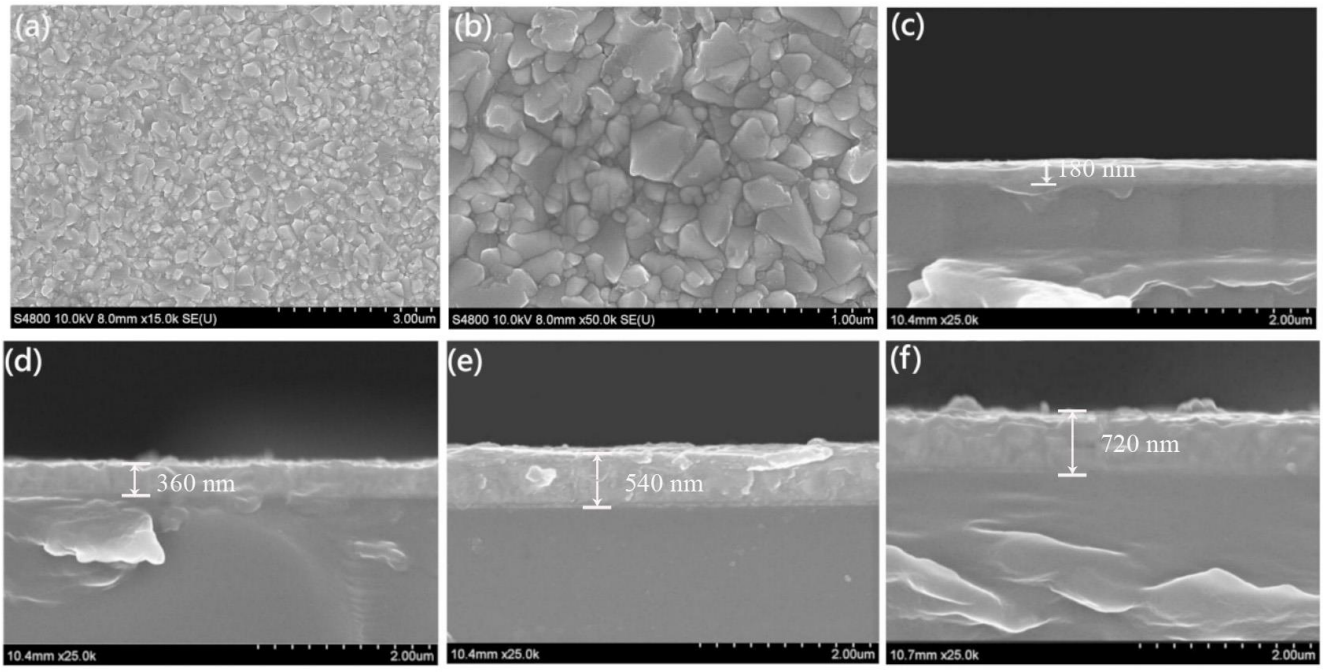

Fig. 3. (a)(b) are for topography images and (c)-(f) are for cross-sectional SEM images of WO_3 film prepared with 15mL, 30mL, 45mL and 60mL peroxotungstic acid precursor solution, respectively

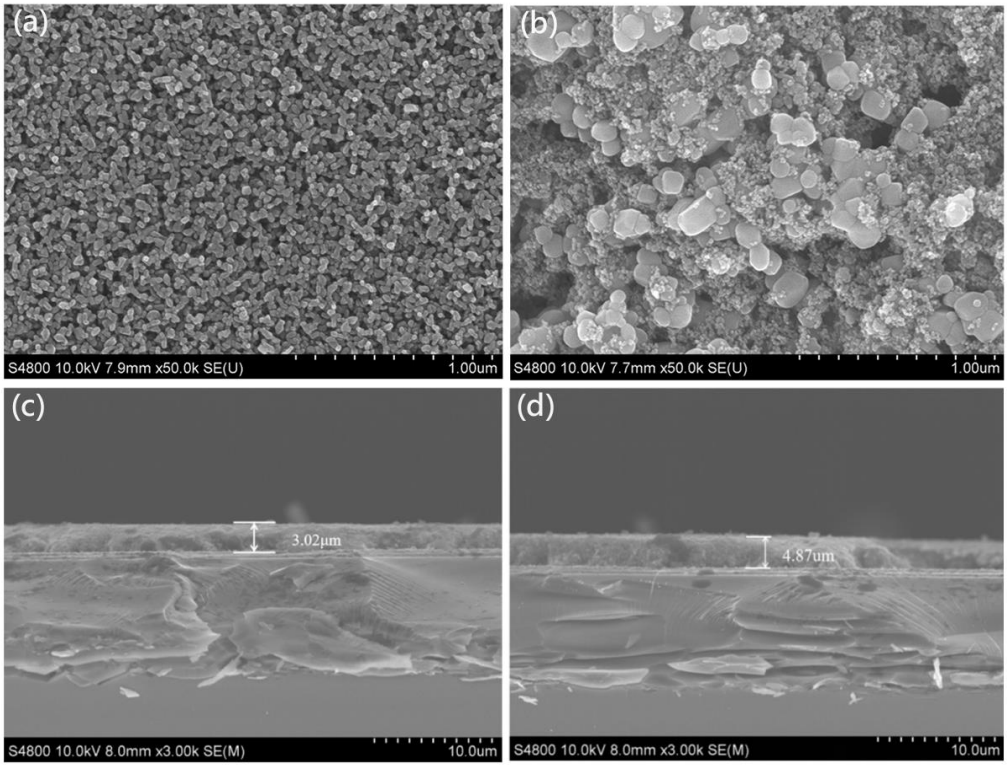

Fig. 4. The SEM images of TiO_2 film. (a)(b) is for top view and (c)(d) is for side view of TiO_2 film without and with scattering layer

Two kinds of TiO_2 pastes were used to prepare photoanode films. Transparent TiO_2 comprising of nanoparticles (with a diameter around 15 nm, shown in Fig. 4a) is beneficial to efficient dye adsorption process, and

light-scattering TiO_2 comprising of nanoparticles (with a diameter around 200 nm, shown in Fig. 4b) plays an important role in reducing light reflection and enhancing light harvesting ability. The cross-sectional images indicated that the thickness for transparent TiO_2 and light-scattering TiO_2 is around 3 μm and 5μm, respectively.

3.2. Optical property

The UV-vis absorption spectra of TG6 adsorbed onto WO_3/TiO_2 composite multi-layer films were performed to investigate the effect on dye adsorption process of WO_3 films. As shown in Fig. 5, a similar absorption profile can be observed for the films, with absorption peaks around 542 nm. The absorption intensity increased along with the increment of WO_3 film, with a ratio of $abs_{without\ WO3}$: $abs_{180nm\ WO3}$: $abs_{360nm\ WO3}$: $abs_{540nm\ WO3}$: $abs_{720nm\ WO3}$ = 2.79:3.12:3.24:3.44:4.08, respectively. Apparently, the introduction of WO_3 film effectively promotes the dye adsorption process, which is beneficial to light harvesting.

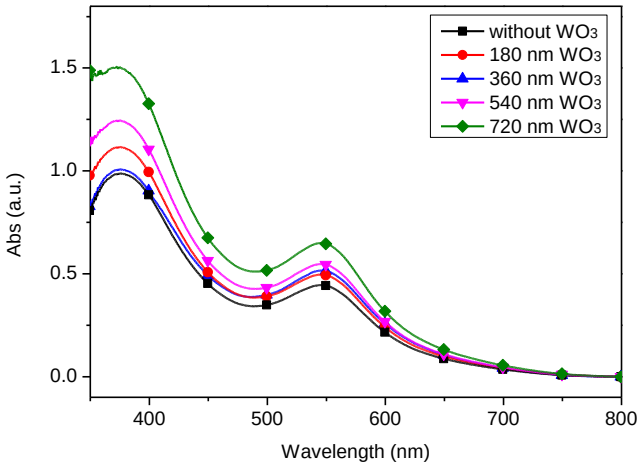

Fig. 5. Absorption spectra of dye molecules absorbed onto the pure TiO_2 film and composite multilayers with different contents of WO_3 (color online)

3.3. Electrochemical impedance analysis

To determine the effect of additional WO_3 layer on the internal electron transfer process, the electrochemical impedance spectroscopy (EIS) measurements of the devices was conducted under dark. Fig. 6 presents the typical Nyquist and Bode plots of DSSCs based on pure TiO_2 photoanode and composite photoanodes. Two semicircles located at relative high and low frequency regions can be observed, corresponding to the transfer process at Pt/electrolyte and $(WO_3)TiO_2$/dye/electrolyte interface, respectively. Some important parameters were obtained by fitting the EIS data with the equivalent circuit (Fig. 6c) using ZSimpWin software. The detailed parameters are shown in Table 1. The electron lifetime can be calculated by formula $\tau=1/(2\pi f)$, where f is the frequency of phase angle peak in Bode diagram. Considering the study focused on the effect of additional WO_3 film on the device performance, the conductive substrate, electrolyte and counter electrodes used were exactly the same material, in good accordance with the similar series resistance and Pt/electrolyte interfacial resistance for the devices. As shown in Fig. 6a and Table 1, the charge transport resistance at photoanode/dye interface and the electron lifetime increased along with the introduction of WO_3 film. The introduction of negative conduction band edge WO_3 film [15] can effectively promote the electron transport process because of the larger charge injection driving force, which is beneficial to the inhibition of charge recombination between photogenerated electrons and I_3^- in the electrolyte. When the thickness of WO_3 film further increased, the values for R_{ct2} and electron lifetime declined again, which can be ascribed to enhanced dye aggregation arose by increment of dye adsorption amounts, as shown in Fig. 5.

Table 1. Parameters obtained by fitting the impedance spectra using the equivalent circuit

Photoanodes	R_s[a] (ohm/cm^2)	R_{ct1}[a] (ohm/cm^2)	C_1[b] (F/cm^2)	R_{ct2}[a] (ohm/cm^2)	C_2[b] (F/cm^2)	τ[c] (ms)
without WO_3	19.44	10.17	0.00002734	75.14	0.0002894	11.58
180nm WO_3	20.21	11.42	0.0004194	94.97	0.0002765	13.12
360nm WO_3	20.87	10.74	0.00007194	85.45	0.0003121	12.37
540nm WO_3	20.01	10.59	0.00002383	60.34	0.0002501	8.74
720nm WO_3	21.64	11.51	0.00005799	51.1	0.000289	6.31

[a] Rs, R_{ct1} and R_{ct2} are the series resistance of DSSCs, charge-transfer resistance at Pt/electrolyte and $(WO_3)TiO_2$/dye/electrolyte interface, and carrier transport within electrolyte, respectively. [b] C_1 and C_2 are the constant phase element for the Pt/electrolyte and TiO_2/dye/electrolyte interface, respectively. [c] τ presents the electron lifetime calculated according to the equation of $\tau=1/(2\pi f)$.

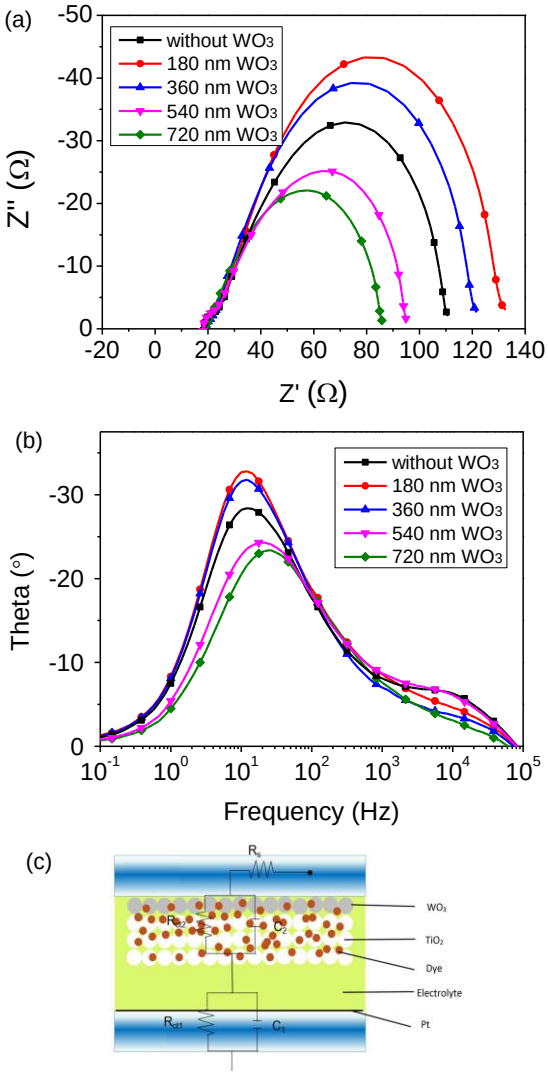

Fig. 6. Nyquist (a) and Bode (b) curves of DSSCs based on pure TiO_2 photoanode and composite photoanodes with different contents of WO_3. (c) is for the equivalent circuit for DSSCs (color online)

3.4. Photovoltaic performance

DSSCs were assemble with pure TiO_2 photoanode and composite multilayer photoanodes to investigate the effect of WO_3 thickness on the photovoltaic performance. Fig. 7 presents *I-V* curves of the cells measured at 100 mW cm^{-2} under simulated AM 1.5G solar light, and the resulting parameters such as short circuit current density (J_{sc}), open circuit voltage (V_{oc}), fill facter (*ff*) and overall conversion efficiency (η) were summarized in Table 2.

Table 2. The detailed photovoltaic parameters of DSSCs based on pure TiO_2 photoanode and composite photoanodes with different contents of WO_3

DSSCs	V_{oc} (mV)	J_{sc} (mA/cm^2)	η (%)	*ff*
without WO_3	674	9.30	3.95	0.63
180 nm WO_3	674	11.32	4.83	0.63
360 nm WO_3	670	12.15	5.05	0.62
540 nm WO_3	666	13.04	5.39	0.62
720 nm WO_3	656	11.75	4.72	0.61

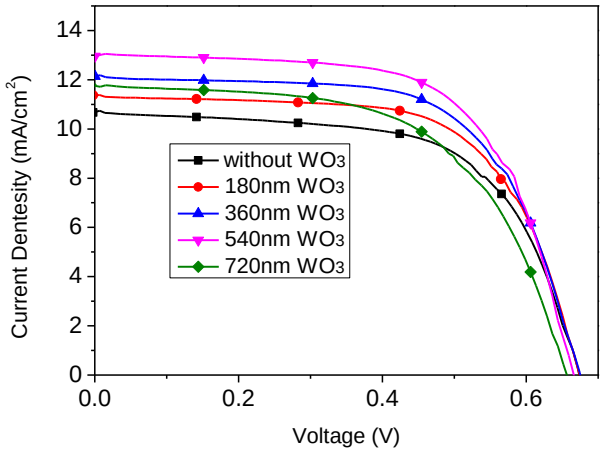

Fig. 7. Photocurrent-voltage curves of DSSCs based on pure TiO_2 photoanode and composite photoanodes with different contents of WO_3

With respect to DSSCs based on pure TiO_2 photoanode, the introduction of WO_3 into the devices significantly enhanced the J_{sc} and η, which can be attributed to a lager dye adsorption amount and relatively larger charge transfer resistance. When the thickness of the WO_3 is further increased to 720 nm, the J_{sc} and V_{oc} of the devices decreased, which can be ascribed to the significant dye aggregation and its relatively small charge recombination resistance as depicted in EIS results. Besides, the theory open circuit voltage for DSSCs can be calculated through the gap between conduction band of electron layer and redox mediam. Considering the more negative conduction band edge of WO_3 film with respect to TiO_2 photoanode, a relatively low theory open circuit voltage for multi-layer photoanodes based DSSCs should be another interfering factor for the decrement of V_{oc}. When a 540 nm WO_3 film was introduced into the photoanodes, an optimized PCE of 5.39% was achieved, accompanied with J_{sc} and V_{oc} of 13.04 mA/cm^2 and 666 mV, respectively.

4. Conclusion

A WO_3/TiO_2 multilayer composite film was developed as electron transporting layer through facile spray pyrolysis to promote interfacial charge transfer process in DSSCs. The results indicated that a compact WO_3 layer with controllable thickness can be obtained through spray pyrolysis method. The introduction of additional WO_3 film was favorable to dye chemadsorption process. Consequently, the short circuit current density was enhanced significantly along with increment of the WO_3 film. Besides, the suitable band gap of WO_3 film can efficiently promote electron injection process, which is beneficial to release electron accumulation in the conduction band of TiO_2 film, thus reduce unfavorable charge recombination. The open circuit voltage decreased again when the WO_3 film further increased to 720nm, which can be ascribed to a decrease in theory open circuit voltage arose by the relatively negative conduction band edge of WO_3. The DSSCs based on 540nm WO_3/TiO_2 hybrid composite film achieved an optimization both in open circuit voltage and short circuit current density with respect to those based on traditional TiO_2 electron transporting layer, an overall PCE of 5.39% was achieved under optimized condition. The results indicated that the modification with additional electron transporting layer is an effective strategy to improve the performance of the DSSCs.

Acknowledgements

The authors gratefully acknowledge the support from the National Natural Science Foundation of China (grant number 51702210) and Gaoyuan Discipline of Shanghai Environmental Science and Engineering (Resource Recycling Science and Engineering).

References

[1] B. O'Regan, M. Grätzel, Nature **353**(6346), 737 (1991).
[2] K. Hu, R. N. Sampaio, J. Schneider, L. Troian-Gautier, G. J. Meyer, J. Am. Chem. Soc. **142**(38), 16099 (2020).
[3] J. W. Gong, K. Sumathy, Q. Q. Qiao, Z. P. Zhou, Renew. Sust. Energ. Rev. **68**, 234 (2017).
[4] S. Mathew, A. Yella, P. Gao, R. Humphry-Baker, B. F. E. Curchod, N. Ashari-Astani, I. Tavernelli, U. Rothlisberger, M. K. Nazeeruddin, M. Grätzel, Nat. Chem. **6**(3), 242 (2014).
[5] A. Yella, H.-W. Lee, H. N. Tsao, C. Yi, A. K. Chandiran, M. K. Nazeeruddin, E. W.-G. Diau, C.-Y. Yeh, S. M. Zakeeruddin, M. Gräzel, Science **334**, 629 (2011).
[6] A. Hagfeldt, G. Boschloo, L. Sun, L. Kloo, H. Pettersson, Chem. Rev. **110**(11), 6595 (2010).
[7] H. Cheema, J. H. Delcamp, Chem-Eur. J. **25**(62), 14205 (2019).
[8] S. Thogiti, J. Y. Park, T. Chau Thi Thanh, D. K. Lee B.-K. Min, H. J. Yun, J. H. Kim, ACS Sustain. Chem. Eng. **6**(10), 13025 (2018).
[9] S. G. Ullattil, S. B. Narendranath, S. C. Pillai, P. Periyat, Chem. Eng. J. **343**, 708 (2018).
[10] G. Nuspl, K. Yoshizawa, T. Yamabe, J. Mater. Chem. **7**(12), 2529 (1997).
[11] X. Gong, Q. Sun, S. Liu, P. Liao, Y. Shen, C. Grätzel, S. M. Zakeeruddin, M. Grätzel, M. Wang, Nano Letters **18**(6), 3969 (2018).

[12] W. Ke, G. Fang, J. Wang, P. Qin, H. Tao, H. Lei, Q. Liu, X. Dai, X. Zhao, ACS Applied Materials and Interfaces **6**(18), 15959 (2014).
[13] P. Zhong, X. Chen, B. Niu, C. Li, Y. Wang, H. Xi, Y. Lei, Z. Wang, X. Ma, J. Power Sources **450**, 227715 (2020).
[14] B. Unlu, M. Ozacar, Sol. Energy **196**, 448 (2020).
[15] H. Abdullah, S. Mahalingam, K. J. Xian, A. Manap; M. H. D. Othman, M. Akhtaruzzaman, Polym. Bull. (2020), doi: 10.1007/s00289-020-03396-w.
[16] S. Ni, F. Guo, D. Wang, S. Jiao, J. Wang, Y. Zhang, B. Wang, P. Feng, L. Zhao, Crystals **9**(2), 113 (2019).
[17] S.-H. Han, W.-Y. Rho, B.-H. Jun, ACS Omega **4**(23), 20346 (2019).
[18] E. Akman, S. Akin, T. Ozturk, B. Gulveren, S. Sonmezoglu, Sol. Energy **202**, 227 (2020).
[19] M. Qamar, B. Zhang, Y. Feng, Opt. Mater. **89**, 368 (2019).
[20] J. Yue, Y. Xiao, Y. Li, G. Han, Y. Zhang, W. Hou, Organic Electronics **43**, 121 (2017).
[21] G. Zhu, H. Wang, Q. Zhang, L. Zhang, J. Colloid Interf. Sci **451**, 15 (2015).
[22] Z. Chen, L. Zhang, Y. Sun, J. Hu, D. Wang, Adv. Funct. Mater. **19**(23), 3815 (2009).
[23] F. Wang, C. Di Valentin, G. Pacchioni, ChemCatChem **4**(4), 476 (2012).
[24] R. A. Dixon, J. J. Williams, D. Morris, J. Rebane, F. H. Jones, R. G. Egdell, S. W. Downes, Surf. Sci. **399**(2), 199 (1998).
[25] Y. Xu, M. A. A. Schoonen, American Mineralogist **85**, 543 (2000).
[26] H. Zhu, W. Li, Y. Wu, B. Liu, S. Zhu, X. Li, H. Agren, W. Zhu, ACS Sustainable Chemistry & Engineering **2**(4), 1026 (2014).

*Corresponding author: wqli@sspu.edu.cn